CEAS-GNC-2024-015

EuroGNC Navigation Guidance Control CEAS Bristol, UK June 11th-13th 2024
University of BRISTOL ROYAL AERONAUTICAL SOCIETY AIAA

Return-to-Home Function for an Integrated Flight Guidance System in Non-Segregated Airspace

Zoe Mbikayi Research Associate, Technical University of Munich, Institute of Flight System Dynamics, 85748, Garching near Munich, Germany. zoe.mbikayi@tum.de

Tim Rupprecht Research Associate, Technical University of Munich, Institute of Flight System Dynamics, 85748, Garching near Munich, Germany. tim.rupprecht@tum.de

Agnes Steinert Research Associate, Technical University of Munich, Institute of Flight System Dynamics, 85748, Garching near Munich, Germany. agnes.steinert@tum.de

Dominik Heimsch Research Associate, Technical University of Munich, Institute of Flight System Dynamics, 85748, Garching near Munich, Germany. dominik.heimsch@tum.de

Florian Holzapfel Head of Institute, Technical University of Munich, Institute of Flight System Dynamics, 85748, Garching near Munich, Germany. florian.holzapfel@tum.de

ABSTRACT

This paper presents a return-to-home function with a turn-around maneuver developed as a part of an automatic trajectory generation system, for an integrated flight guidance system. The trajectory generation system has been developed at the Institute of Flight System Dynamics as a modular and flexible platform that can be used for a broad range of systems. The turn-around maneuver presented in this paper is based on a 45°/180° procedure turn, which is used to reverse the course of the aircraft, before flying the inverted flight plan in order to go back to the take-off point. The decision to invert the flight plan is motivated by the fact that the system is intended to be used in non-segregated airspace, where the aircraft might not be allowed to simply fly a straight line or an optimized path other than the uploaded flight plan. The paper presents both the development of the maneuver, and the integration logic in the trajectory generation system.

Keywords: GNC; eVTOL; Return-to-home; Trajectory Generation; Flight Guidance

Nomenclature

WP	=	Waypoint
$\phi_{WP_n}, \lambda_{WP_n}$	=	Latitude and Longitude of waypoint n
d_{m,WP_n}	=	Euclidean Distance from WP_{n-1} to WP_n in meters
ρ_{WP_n}	=	Radian distance from WP_{n-1} to WP_n in radians considering spherical geometry
r_{earth,WP_n}	=	Radius of the earth calculated at WP_n

1 Introduction

The development of advanced integrated flight guidance systems has become a critical area of research in modern aviation. This is because of the particularly increasing emphasis on autonomy and safety, given the planned and on-going integration of Unmanned Aerial Systems (UAS) and Optionally Piloted Vehicle (OPV) in the non-segregated airspace [1]. Online trajectory generation, together with trajectory optimization, play a crucial role in ensuring accurate and dynamic, flight planning and control, and has been used in several instances, especially for obstacle avoidance [2]. Recent literature on online trajectory generation has demonstrated various approaches to the main problem of trajectory generation, addressing challenges such as obstacle avoidance [3], flight efficiency [4, 5], compliance with operational constraints [6, 7] and optimization of trajectories considering airspace constraints and regulatory requirements [8]. One of the most common things among all the different approaches, is that the easiest way and most efficient way to make a trajectory from point A to point B, is to use a straight line. This is equivalent to the arc of a great circle in case of the shortest path on the surface of a sphere or spheroid. In the case where there are constraints that need to be satisfied along the trajectory, the shortest path is made of straight lines and circular arcs. This was demonstrated in [9] where the author showed when the orientation at the start and end point is specified as a constraint, the shortest path is constructed by a combination of straight lines and circular-arcs. This approach was later extended to the 3D problem, and the solution remains similar [10]. It is evident here that connecting a straight line to a circular arc will produce a discontinuity in the curvature of the trajectory given that a straight line has a curvature of $\kappa = 0$, while a circle has a curvature inversely proportional to its radius, such that of $\kappa = 1/r$. This implies that when the aircraft is at the junction of the line and circular arc, the required bank angle has a discontinuity, in order to follow the trajectory. This problem is solved by adding transition curves that are developed using several approaches, such as Bezier curves ([11–13]), and clothoids / Euler spirals ([14–17]). Even though the problem of online trajectory generation is widely researched, the integration of a return-to-home function, or development of course reversal maneuvers and other terminal airspace maneuvers has received limited attention. The present paper is an extension to the system developed in [15] and focuses on the design and implementation of a turn-around maneuver. This can be used for course reversal in terminal airspace or for a return-to-home function, which is the current application. The system is incorporated and tested in an integrated flight guidance system similar to [18]. In the event of a return-to-home request, this maneuver allows the aircraft to execute a smooth and deterministic turn, before inverting the flight plan from the most recent waypoint and guiding the aircraft back to its take-off point. The turn around maneuver is based on a 45-degree/180-degree procedure turn as prescribed by the International Civil Aviation Organization (ICAO) [19]. The function, as presented, has a maneuver planning module which dynamically calculates the required waypoints for the turn-around maneuver, ensuring that the aircraft can execute the maneuver safely and efficiently, regardless of its current position and speed. The maneuver is augmented with a state-flow logic to enable seamless integration with the integrated flight guidance system.

2 Maneuver Planing

2.1 Integrated flight guidance system

The overview of the integrated flight guidance system is given in Figure 1. This integrated system has been flown and tested with different types of inner loop controllers and different aircraft configurations, including fixed-wing, eVTOL, and currently is being integrated into the Avilus MEDEVAC multicopter [20–22].

The different modules depicted in Figure 1 are:

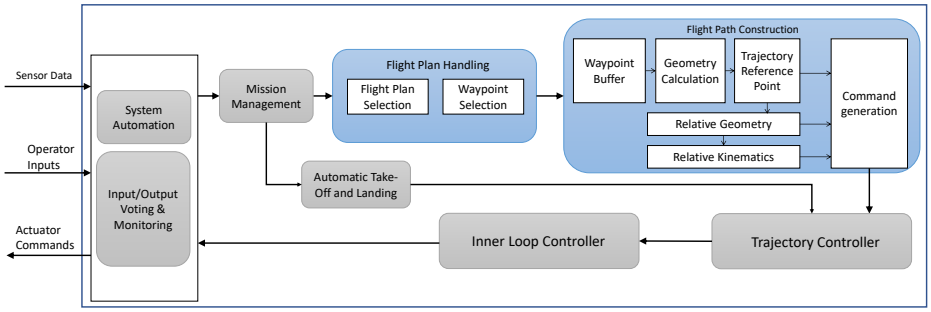

Fig. 1 Integrated flight guidance system overview

2.1.1 System Automation

This is the main decision-making module, which decides which other modules needs to be activated and when. It is responsible for activating the trajectory generation system after take-off, or when requested by the operator. This is done by introducing operational sequence diagrams that represent the procedural system behavior, in order to describe the scenarios of the concept of operations. This module is based on the work in [23].

2.1.2 Inputs/Outputs Voting and Monitoring

This module performs signal integrity and validity checks for all the input/output data. Additionally, in case of redundant signals, the module performs signal voting [24].

2.1.3 Mission Management

This module is responsible for flight plan data handling [25] and geofencing function [26]. Each waypoint in the flight plan is characterized by an ID, the WGS84 position coordinates including altitude, the kinematic speed command, the ARINC-424 leg type [27] (track-to-fix, or radius-to-fix), and three custom fields. In case of a track-to-fix leg, the custom fields contain the type of transition, which can be either fly-by or fly-over. In case of a radius-to-fix leg, the custom fields contain the WGS84 longitude and latitude coordinates of the radius-to-fix circle center, and the turn direction of the maneuver.

2.1.4 Automatic Take-Off and Landing

This module performs automatic take-offs and transitions from hover to cruise flight in the direction of the first waypoint in the flight plan. It is then deactivated once the aircraft has reached a certain defined minimum speed for the trajectory generation system. This module also performs the transitions from cruise to hover and landings. It is based mainly on the work in [28] and was flight tested on a light all electric optionally piloted aircraft [29].

2.1.5 Flight Plan Handling

This is a sub-module of the trajectory generation system, which selects the correct flight plan, and decides which waypoint should be sent to the flight path generation sub-module [25].

2.1.6 Flight Path Construction

This module is responsible for all the calculations needed to construct the flight path. It includes a waypoint buffer, which always contain four waypoints, three of which are necessary for the construction of the trajectory, and one, which is in the buffer for safety and can be modified by the flight plan handling module. The outputs are the feedforward commands and the error dynamics up to jerk level [25, 30].

2.1.7 Trajectory Controller

This module receives the feedforward commands and error dynamics computed by flight path construction sub-module, and solves the trajectory control problem. The outputs are the commands used in the inner loop. This module is mainly based on the work in [31] and [20].

2.1.8 Inner Loop Controller

This is the most inner module of the flight control system, which generates the commands that are directly applied to the actuators of the aircraft [32, 33]. The proper functioning of the inner loop controller is crucial for all other modules in Figure 1 to operate correctly. The flight guidance system can be applied to different inner loop controller modules, which allow for the interfaces described in [34].

It is worth noting that only the flight plan handling and flight path construction modules are of interest in the framework of online trajectory generation.

2.2 Course reversal maneuver

The DOC 8168 presents four course reversal procedures to be used, usually in terminal airspace [19]. Considering that we want to reverse the course and return on the same track, all while maintaining the smallest deviation from the original trajectory, the only viable choices are the 45°/180° and the 80°/260° procedure turns. The latter takes the least deviation, however, the former is the simplest. Therefore, as a proof of concept, the 45°/180° maneuver, as shown in Figure 2, was selected for the return-to-home function. A limitation of the approach is that even though the deviation is minimized, the aircraft still deviates from the approved trajectory. A possible fix to this problem is to include the space required for a turn-around maneuver in the original flight trajectory approval procedure and perform the maneuver at minimum speed. The procedure turn is described as follows:

> The 45°/180° procedure turn starts at a facility or fix and consists of:
>
> 1) a straight leg with track guidance. This straight leg may be timed or may be limited by a radial or distance measuring equipment (DME) distance;
> 2) a 45° turn;
> 3) a straight leg without track guidance. This straight leg is timed. It is:
>   1) 1 minute from the start of the turn for Category A and B aircraft; and
>   2) 1 minute 15 seconds from the start of the turn for Category C, D and E aircraft; and
> 4) a 180° turn in the opposite direction to intercept the inbound track. *[19]*

As can be seen above the 45°/180° procedure turn depends on the aircraft category. For this application the aircraft category is determined based on the planning speed, i.e. the speed that is used to plan the maneuvers. The calculation of the planning speed is explained in section 3. Additionally, the waypoints are set at the altitude of the aircraft at the moment when the procedure turn is requested.

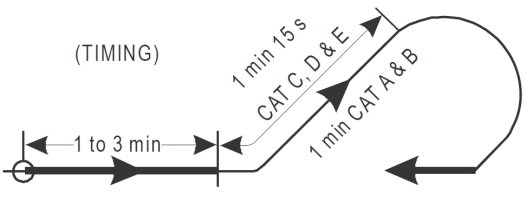

Fig. 2 45°/180° **procedure [19]**

To plan the maneuver, a total of four waypoints are computed as shown in Figure 3. These waypoints are continuously generated from the current aircraft position, in order to ensure the maneuver is available at anytime, when requested. This request would be allowed only if the aircraft is not in a turn/ transition maneuver, and is flying in a straight line. This will guarantee that in the reversed flight, the aircraft will always be able to proceed the most recent turn maneuver. It is also worth noting that each waypoint is

a function of the previous waypoint, with the first waypoint being a function of the aircraft position as shown later.

2.3 Geometry calculations

The maneuver is planned geometrically as shown in Figure 3, where all the geometrical calculations are performed under the assumption that the earth is a perfect WGS84 ellipsoid. These calculations are part of the flight plan handling module.

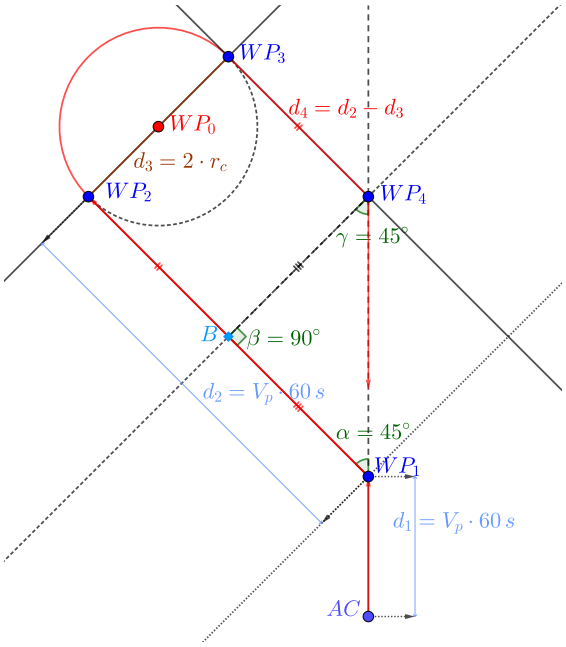

Fig. 3 Maneuver geometry

Given a waypoint WP_1 defined by its longitude λ_{WP_1}, latitude ϕ_{WP_1} and altitude h_{WP_1}, a second waypoint WP_2 at a course angle χ_{WP_1,WP_2} and distance d_{m,WP_2}, defined by its latitude and longitude can be computed as follows:

- First, the distance from WP_1 to the center of earth r_{earth,WP_1} is calculated using the Euler law for surface curvatures as follows [35]:

$$r_{earth,WP_1} = \frac{1}{\left(\frac{1}{N_m} - \frac{1}{M_m}\right) \cdot \sin^2\left(\chi_{WP1,WP_2}\right) + \frac{1}{M_m}}, \tag{1}$$

where N_m is the prime vertical radius of the WGS84 ellipsoid at the location of WP_1 plus the altitude of the waypoint, and M_m is the meridian radius plus the altitude of the waypoint [36]:

$$N_m = \frac{a}{\sqrt{1 - e^2 \cdot \sin\left(\phi_{WP_1}\right)}} + h_{WP_1}, \tag{2}$$

$$M_m = \frac{a(1 - e^2)}{\sqrt{\left(1 - e^2 \cdot \sin\left(\phi_{WP_1}\right)\right)^3}} + h_{WP_1}, \tag{3}$$

where $a = 6378137\ m$ is the semi-major axis, $e = \sqrt{f(2 - f)}$ is the eccentricity and $f = 1/298.257223563$ is the flattening of the WGS84 ellipsoid.

Since χ_{WP_1,WP_2} might not point exactly in the direction of χ_{WP_2,WP_1} because of the ellipsoid characteristics of the earth, the usual approach is to calculate the earth radius at both waypoints, with their respective course angle, and take the mean between both. However, in our case, we do not have the second waypoint. But given the small distances involved, the ellipsoidal effects can be assumed to be negligible. In addition, calculating the radius of the earth using this perfect sphere assumption leads to numerical errors that have been shown to correspond to a maximum error of $\pm 42\ m$ for distances up to $1000\ km$ [25].

- In the second step, the radian distance ρ_{WP_2} is calculated. This is the angle it takes to travel along an arc with length d_{m,WP_2} of a great circle from WP_1 to WP_2, i.e. $\rho_{WP_2} \cdot r_{earth,WP_1} = d_{m,WP_2}$. Hence, the radian distance is calculated by

$$\rho_{WP_2} = \frac{d_{m,WP_2}}{r_{earth,WP_1}}, \tag{4}$$

Note that the distance d_{m,WP_2} is assumed to be in a range such that r_{earth,WP_1} is approximately equal to r_{earth,WP_2}, and the WP_2 is placed at the same altitude as WP_1.

- The third step is to fix the singularities that can occur in the course angle at the north and south poles. This is done as follows:

if $\phi_{WP_1} = \frac{\pi}{2}$ (North pole) **then**
  $\chi_{WP_1,WP_2} = \pi$
else if $\phi_{WP_1} = -\frac{\pi}{2}$ (South pole) **then**
  $\chi_{WP_1,WP_2} = 2\pi$
end if

- The fourth step is the calculation of the latitude of the second waypoint, ϕ_{WP_2}, as follows:

$$\begin{aligned} \phi_{WP_2} = \arcsin \big[& \cos\left(\rho_{WP_2}\right) \cdot \sin\left(\phi_{WP_1}\right) + \\ & \sin\left(\rho_{WP_2}\right) \cdot \cos\left(\chi_{WP_1,WP_2}\right) \cdot \cos\left(\phi_{WP_1}\right) \big] \end{aligned} \tag{5}$$

- The fifth step is the calculation of the absolute value of the longitude change $\left|\Delta\lambda_{WP_1,WP_2}\right|$:

if $\cos\phi_{WP_2} \cos\phi_{WP_1} = 0$ **then**
  $|\Delta\lambda_{WP_1,WP_2}| = 0$
else
  $|\Delta\lambda_{WP_1,WP_2}| = \arccos\left(\frac{\cos\rho_{WP_2} - \sin\phi_{WP_2}\sin\phi_{WP_1}}{\cos\phi_{WP_2}\cos\phi_{WP_1}}\right)$
end if

- The sixth step is the determination of the sign of $\Delta\lambda_{WP_1,WP_2}$:

if χ_{WP_1,WP_2} is in range $[0, \pi)$ **then**
  $\text{sign}(\Delta\lambda_{WP_1,WP_2}) = 1$
else
  $\text{sign}(\Delta\lambda_{WP_1,WP_2}) = -1$
end if

- The last step is the calculation of the longitude:

if $\text{sign}(\Delta\lambda_{WP_1,WP_2}) = 1$ **then**
  $\lambda_{WP_2} = \lambda_{WP_1} + \left|\Delta\lambda_{WP_1,WP_2}\right|$ flipped in range $(-\pi, \pi]$
else
  $\lambda_{WP_2} = \lambda_{WP_1} - \left|\Delta\lambda_{WP_1,WP_2}\right|$ flipped in range $(-\pi, \pi]$
end if

The calculations above represent an analytical solution to the direct geodesic problem, and are compiled into a common geometrical calculations function which takes as arguments, an initial waypoint with its parameters: longitude, latitude, altitude, course angle to the second waypoint, χ_{WP_1,WP_2}, and the distance, d_{m,WP_2} to the second waypoint in meters. The four waypoints of the procedure turn maneuver, as depicted in Figure 3, are then computed as using the parameters shown in table 1. Note that the 60 seconds used in the table reflect the category A of the aircraft from [19], and χ_{WP_x} is used to depict the course angle that the aircraft would need in order to reach WP_x from WP_{x-1}.

Table 1 Waypoint parameters

WP_x	WP_{x-1}	χ_{WP_{x-1},WP_x}	d_{m,WP_x}
WP_1	WP_{ac}	$\chi_{WP_{ac}}$	$d_1 = V_p \cdot 60\,sec$
WP_2	WP_1	$\chi_{WP_1} - 45°$	$d_2 = V_p \cdot 60\,sec$
WP_3	WP_2	$\chi_{WP_2} + 90°$	$d_3 = 2 \cdot r_c$
WP_4	WP_3	$\chi_{WP_3} + 90°$	$d_4 = d_2 - d_3$

where V_p is the planning speed defined in section 2.2, and $r_c = 1.5 \cdot V_p/\dot{\chi}$ is the radius of a hypothetical turn that the aircraft could do, given the planning speed and a predefined maneuver turn rate $\dot{\chi}$, with a margin of 50 % to account for the build up of the bank angle for the turn.

2.3.1 Waypoint 1

This waypoint is placed directly in front of the aircraft, and therefore the course angle to the waypoint is the same as that of the aircraft at the moment when the procedure turn is requested. The distance is defined such that the aircraft completes the leg in 60 seconds. This distance can be adjusted for different aircraft categories. The waypoint is defined with a fly-by transition and track-to-fix leg type.

2.3.2 Waypoint 2

This waypoint is placed at a distance of $V_p \cdot 60$ seconds, and with an angle of 45° between the $[WP_1 - WP_2]$ leg and $[AC - WP_1]$ leg, to the left of the latter. The waypoint is defined with a fly-over transition and track-to-fix leg type.

2.3.3 Waypoint 3

This waypoint is placed at a distance equivalent to the diameter of a circle from waypoint 2, with a course angle change of 90° to the right. This waypoint is specified as having a radius-to-fix leg type. The radius-to-fix maneuver starts at WP_2 and ends at WP_3. The position of the radius-to-fix circle center, WP_0, is calculated the same way as WP_3, but at half of the distance.

2.3.4 Waypoint 4

This waypoint is placed at a 90° course change to the right of WP_3, and is defined as the intersection of the initial inbound leg and the line which is perpendicular to the $[WP_2 - WP_3]$ leg, at WP_3. This intersection point can be found by computing the different distances and angles involved in the maneuver as follows (the illustration of the following postulates and procedures can be seen in Figure 3, and it is assumed that the 3D space is projected onto a horizontal plane, and therefore the altitude is not used):

- We place a line parallel to the $[WP_2 - WP_3]$ leg, and passing through WP_4. This line will cross the $[WP_1 - WP_2]$ leg at point B with an angle $\beta = 90°$. This creates a triangle $\triangle[WP_1 - B - WP_4]$, with angles α, β and γ.

- β is 90 ° because $[WP_1 - WP_2]$ has a 90 ° intersection angle with $[WP_2 - WP_3]$. And by the corresponding angles postulate, which states, *if two parallel lines are cut by a transversal, then the corresponding angles are congruent* [37], we can deduce that β must be 90 °. And since the sum of angles in a triangle add up to 180 °, γ must necessarily be equal to 45 °.

- *If in a triangle two angles be equal to one another, the sides which subtend the equal angles will also be equal to one another* [38, 39]. Since α and γ are equal, the sides of the triangle must also be equal. Therefore, the side $[B - WP_1]$ is equal to $[B - WP_4]$, which is also equal to $[WP_2 - WP_3]$, which is itself known ($d_3 = 2 \cdot r_c$).

Therefore, it follows from the postulates above, that, the distance $[WP_3 - WP_4]$ is $d_4 = d_2 - d_3$. This distance is then used to compute waypoint 4. This waypoint is defined as a track-to-fix with a fly-by transition.

These four waypoints are compiled into a flight plan, which can be used for the external maneuver as described in section 4.

Note that another approach is to project the waypoints and make the calculations above in a local Cartesian frame before projecting them back into the WGS84 frame. However, as shown in [25], this kind of transformation needs to be done in two steps, using the Earth-Centered, Earth-Fixed (ECEF) frame as intermediary. This introduces small numerical errors. Given the short distances involved in the maneuver, the WGS84 coordinates of the waypoints require all the numerical precision that can be afforded. Doing the geometrical calculations in the WGS84, although computationally expensive, enables the system to maintain good accuracy.

3 Online Trajectory Generation

The online trajectory generation module, as highlighted in Figure 1, is mainly based on the work in [25]. As described in the previous section, the procedure turn maneuver requires fly-by and fly-over transitions, and one radius-to-fix leg type. To plan these maneuvers, the planning speed V_p is used. This is calculated as shown in equation (6). The goal is to use the highest velocity that the aircraft might reach during the maneuver. Hence, the maximum between the commanded kinematic speed and measured kinematic speed. Additionally, there is a buffer velocity of $5m/s$ added to account for uncertainty. This is because a maneuver planned with a higher speed will always be achievable if the actual speed of the aircraft is lower and not vice versa.

$$V_p = \max(V_K, V_{K,cmd}) + V_{K,buffer} \tag{6}$$

The online-generated trajectory is only defined and characterized by a trajectory reference point. This point is defined as the point on the hypothetical reference trajectory with the smallest distance to the aircraft. Therefore, both the feedforward commands and error dynamics, are generated as a function of the current trajectory reference point, and the current aircraft states. The velocity commands however, are directly transmitted from the velocity property of the waypoint toward which the aircraft is flying.

3.1 Transition segments

As described in the introduction, the maneuvers are designed by combining straight line segments with circular arc segments. Therefore, transition segments are needed in order to avoid curvature discontinuities in the trajectory. Clothoid segments are used for this. Details about clothoid transitions can be found in [25]. In general, clothoids are represented by Fresnel integrals as shown in equation (7).

$$\begin{bmatrix} x_{cl}(\tau) \\ y_{cl}(\tau) \end{bmatrix} = \begin{bmatrix} x_i + A \cdot \int_{k=0}^{\tau} \cos\left(k^2\right)\ \mathrm{dk} \\ y_i + A \cdot \int_{k=0}^{\tau} \sin\left(k^2\right)\ \mathrm{dk} \end{bmatrix} \tag{7}$$

Given the real-time aspect of the module, the analytical solution implemented is an approximation of the integrals using a 5th order power series given in equation (8).

$$\begin{bmatrix} x_{cl}(\tau) \\ y_{cl}(\tau) \end{bmatrix} = \begin{bmatrix} x_i + A \cdot \sum_{m=0}^{5} \frac{(-1)^m}{(2m)!\cdot(4m+1)} \cdot \tau^{4m+1} \\ y_i + A \cdot \sum_{m=0}^{5} \frac{(-1)^m}{(2m+1)!\cdot(4m+3)} \cdot \tau^{4m+3} \end{bmatrix}, \tag{8}$$

where τ is the clothoid running parameter and A is the shaping parameter of the clothoid. This is in fact, the only parameter required for the implementation of the transition segments, and can be parametrized in terms of the performance of the aircraft.

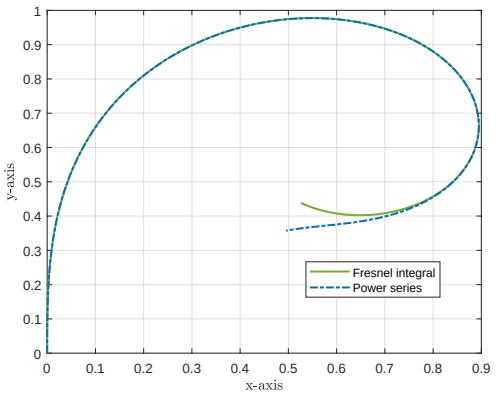

Fig. 4 Fresnel integral vs power series approximation

Figure 4 shows a comparison of the Fresnel integral and the power series comparison. As it is seen, even for cases when the curve has made a full 180 turn, the approximation is still accurate.

The clothoid shaping parameter A can be calculated by:

$$A = \sqrt{\left(4 \cdot T_p + 2 \cdot \frac{\mu_{cmd}}{p_{cmd}}\right) \cdot V_p \cdot r_c}, \tag{9}$$

where r_c is the radius of the maneuver circle, T_p is the roll time constant of the vehicle, essentially describing how long it would take the aircraft to build up a certain bank angle μ_{cmd} which, in this case, is calculated based on the planning speed V_p, and a desired maneuver turn rate $\dot{\chi}$, and p_{cmd} is the desired roll rate, which can be the maximum operational roll rate of the aircraft, or based on the limits applied by the inner loop controller.

3.2 Fly-by transition

A fly-by transition is made of three different sections: A turn-in, circle arc, and turn-out maneuvers. The turn-in and turn-out maneuvers consist of the clothoid transitions. A graphical overview is shown in Figure 5.

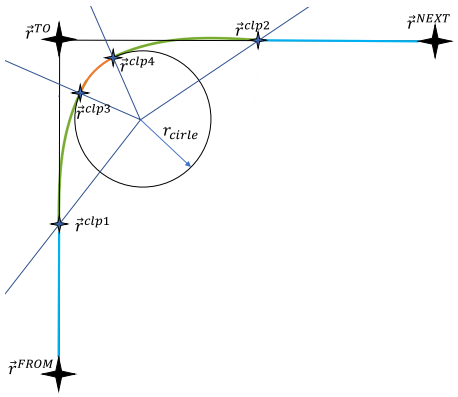

Fig. 5 Fly-by maneuver geometry

3.3 Radius-to-fix leg type

The radius-to-fix leg type, very much like the fly-by, consists of a turn-in, circle arc, and turn-out maneuvers. The turn-in starts at the first waypoint of the maneuver, which should be a fly-over waypoint, and the turn out ends at the second waypoint of the maneuver. The complete maneuver description is presented in [40], and a graphical overview is shown in Figure 6.

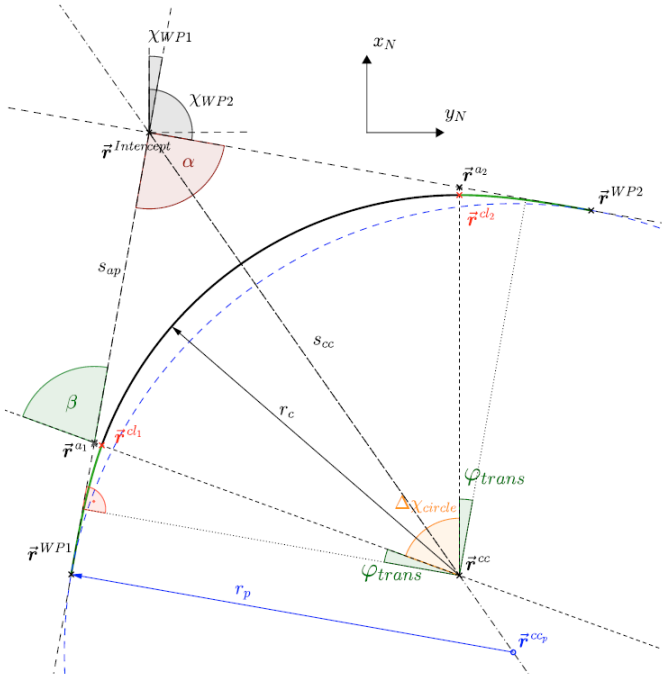

Fig. 6 Radius-to-fix leg type geometry [40]

4 System Integration

The integration of the procedure turn maneuver and reversal function into the whole flight guidance system is mainly accomplished in the flight plan handling unit (FPU), which takes an immediate reversal request from the system automation module. The trajectory generation system can be put in different states as shown in Figure 7. When an immediate reversal is requested, the system goes in a temporary state waiting for an external maneuver to be allowed. This permission comes when the aircraft is flying in a straight line, and not performing any type of turn or climb maneuver. Then the system requests the external maneuver mode, which is described later in this section, and enters the next state. When the FPU sends the last waypoint of the external maneuver, which is the procedure turn in this case, the "start reversal" state is activated. In this state, the FPU starts sending waypoints from the original flight plan to the waypoint buffer (see Figure 1) in the reverse order. If, in reverse mode, the system encounters a radius-to-fix leg, the reverse logic will invert the direction and waypoints of the maneuver. In addition, the altitudes of the reversed trajectory are kept the same as the original trajectory. This assumes a symmetry between the climb and descent performance, which is usually the case for multicopter-type of aircraft.

After finishing the last leg of the procedure turn, the system gets in the "reversal mode". Note that the reversal mode can be canceled only in the "immediate reversal requested" and "reversal mode" states. If the reversal is canceled in an other state in between, then the request will be held until the "reverse mode" is active.

The FPU is split into two modes: the nominal mode and the external mode, which is the turn-around maneuver. The nominal mode is activated when a flight plan is filed for the first time, and the buffer is filled in a serial way as shown in [25]. When the return-to-home function is requested, the system goes in a temporary state waiting for the external maneuver (i.e. turn-around maneuver) to be allowed. This permission comes when the aircraft is flying in a straight line and not performing any type of turn or climb maneuver.

When the external maneuver mode is allowed, the external flight plan of the turn-around maneuver, as described in section 2.2, is uploaded. This clears the waypoint buffer and refills it with the new flight plan. The system enters the external maneuver mode and performs the turn-around. Since the first

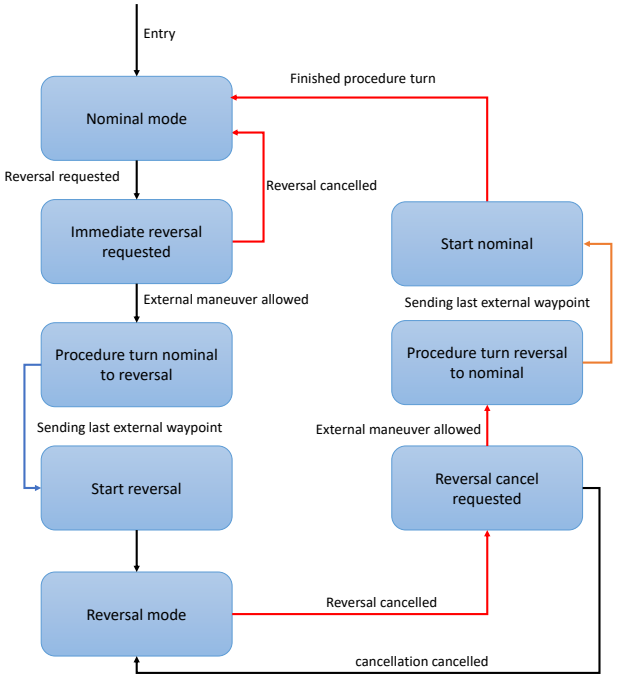

Fig. 7 Top level reversal states flow

waypoint of the turn-around maneuver is placed directly in front of the aircraft, there is no jump in the commands, and the flight remains smooth.

When the FPU sends the last waypoint of the procedure turn, the system enters the "reversal mode" and the "start reversal" state is activated. In this state, the FPU starts sending waypoints from the original flight plan to the waypoint buffer (see Figure 1) in the reverse order, by simply appending the original flight plan in the reverse order to the external maneuver flight plan. This will result in a smooth flight because the last waypoint of the procedure turn is placed directly in line with the last visited waypoint of the original flight plan. If, in reverse mode , the system encounters a radius-to-fix leg, the reverse logic will invert the direction and waypoints of the maneuver. Note, that the reversal mode can be canceled only in the "immediate reversal requested" and "reversal mode" states. If the reversal is canceled in any other state in between, then the request will be held until the "reverse mode " is active. In the case when the reversal is canceled, the system will again perform a procedure turn to reverse the course, and then continue with the original flight plan from the point that it had reached in reverse mode.

5 Results

The system is tested on the Avilus MEDEVAC multicopter, which is an aircraft for medical evacuation (see Figure 8). The implementation was done in Simulink®, following strict modeling guidelines to produce a code compliant software according to DO-178/DO-331 standards [41]. The figures below depict the results of the testing done on the system presented in the paper. These tests were done with the whole flight guidance system, including the inner loop controller, trajectory generation and trajectory controller.

Figure 9 shows the flight plan that was filed in green, and the aircraft position measurements throughout the flight. For the first leg of the flight, the flight plan (in green) is not in the plot as the aircraft is flying from the take-off location to the first waypoint.

Figure 10a shows another flight on the same path, and this time, an immediate return was requested, and the system engaged the turn around function before reversing the flight plan, following the same

Fig. 8 Avilus MEDEVAC Aircraft

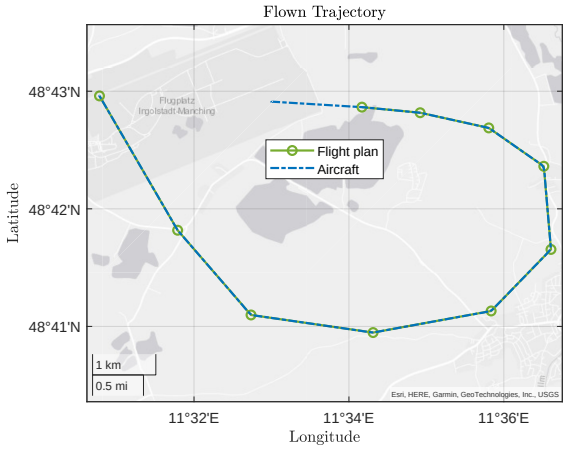

Fig. 9 Nominal flight

path that was taken for the nominal flight. A close-up of the turn around maneuver itself can be seen in Figure 10b.

As it can be seen, after the maneuver is requested, it gets activated immediately since the aircraft was flying in a straight line.

The first 45 ° left turn is achieved automatically by simply specifying that waypoint with a fly-by transition, leading to the second waypoint which is located to the left of the inbound leg. The second turn of the maneuver happens after reaching the second waypoint of the procedure turn, and requires the aircraft to make a 180 ° course change. This is done by performing a radius-to-fix, where the exit angle is the 180 ° course change. This last turn puts the aircraft on a course of intercept with the inbound leg from when the reversal was requested. After reaching the interception point, the aircraft then makes a right turn outbound for the waypoint that came right before the reversal was requested. This is followed by the reversed flight plan, flying back to the base. Hence the turn around functionality works as intended and as described in section 2.3.

A non-nominal case is shown in Figure 11. In sub-Figure 11b, we see in the upper figure, the moment at which the return-to-home function is requested, i.e. when the green line changes from "inactive" to "active". At this moment, however, the aircraft is in a flyby, which is a turn maneuver as we can see in the lower figure, where the active mode is shown. Therefore the procedure turn maneuver is not allowed until the aircraft returns in a straight line, therefore we see that the blue dashed line in the upper figure, representing the status of the procedure turn, remains in "inactive". In sub-Figure 11a, we see the moment at which the reversal is engaged, represented by the orange circle, and followed by a procedure turn before engaging in the flight plan reversal. During the reversal flight, the return-to-home function was canceled,

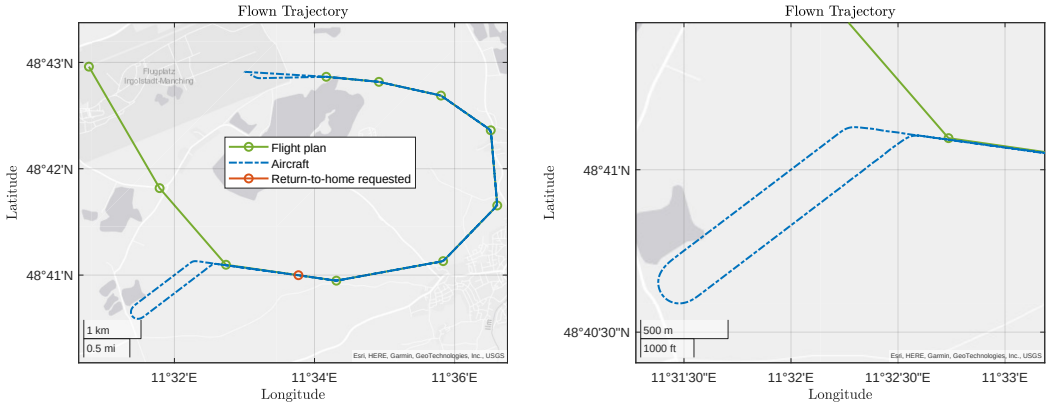

(a) Flight with reversal **(b) Turn around maneuver**

Fig. 10 Flight plan reversal

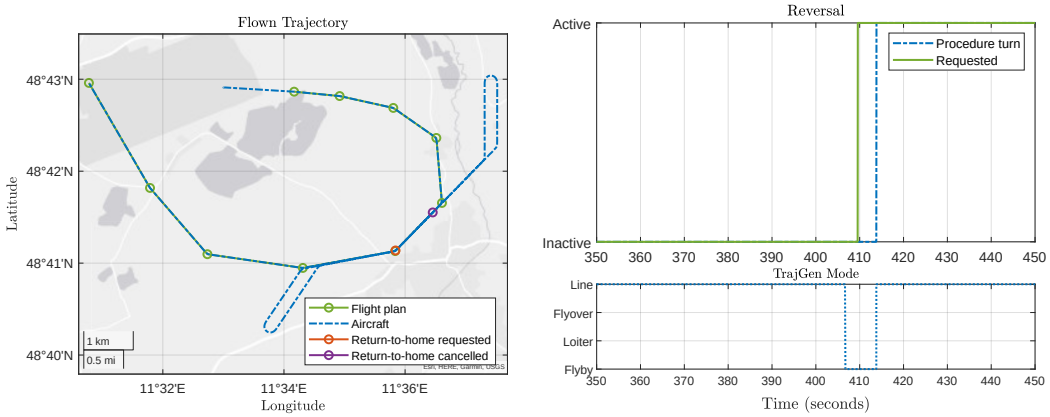

(a) Canceled reversal **(b) Internal moding**

Fig. 11 Non-nominal flight

represented by the purple circle. As seen in Figure 11a, the aircraft goes into another procedure turn, before re-engaging in the flight plan from its current location, proceeding to the closest waypoint.

6 Conclusion

This paper went through the development of a turn-around maneuver for an integrated flight guidance system. the turn-around maneuver is developed to be used in a return-to-home function in non-segregated airspace. Therefore it is paired with a flight plan reversal logic. The turn around maneuver itself is based on the 45°/180° procedure turn used by pilots for course reversal. Several waypoints are generated, with both track-to-fix and radius-to-fix leg types, and fly-by and fly-over transitions. The paper describes the geometrical calculations needed to plan the maneuver, the generation of the waypoints needed, the online generation of the reference trajectory, and the integration of the turn-around maneuver, and return-to-home function in the flight guidance system as a whole. The presented algorithms were implemented in Simulink®, as code compliant software according to DO-178/DO-331 standards [41]. Simulation results including the whole flight guidance system, consisting of inner loop controller, trajectory generation and trajectory controller demonstrate the discussed functionalities.

References

[1] Reece A Clothier, Brendan P Williams, and Neale L Fulton. Structuring the safety case for unmanned aircraft system operations in non-segregated airspace. *Safety science*, 79:213–228, 2015. DOI: 10.1016/j.ssci.2015.06.007.

[2] Chi-Kin Lai, Mudassir Lone, Peter Thomas, James Whidborne, and Alastair Cooke. On-board trajectory generation for collision avoidance in unmanned aerial vehicles. In *2011 Aerospace Conference*, pages 1–14. IEEE, 2011. DOI: 10.1109/AERO.2011.5747526.

[3] Enrique Aldao, Luis M González-deSantos, Humberto Michinel, and Higinio González-Jorge. Uav obstacle avoidance algorithm to navigate in dynamic building environments. *Drones*, 6(1):16, 2022. DOI: 10.3390/drones6010016.

[4] Haichao Hong, Patrick Piprek, Matthias Gerdts, and Florian Holzapfel. Computationally efficient trajectory generation for smooth aircraft flight level changes. *Journal of Guidance, Control, and Dynamics*, 44(8):1532–1540, 2021. DOI: 10.2514/1.G005529.

[5] Angel Romero, Robert Penicka, and Davide Scaramuzza. Time-optimal online replanning for agile quadrotor flight. *IEEE Robotics and Automation Letters*, 7(3):7730–7737, 2022. DOI: 10.1109/LRA.2022.3185772.

[6] Patrick Piprek. *Robust trajectory optimization applying chance constraints and generalized polynomial chaos*. PhD thesis, Technische Universität München, 2020.

[7] Boyu Zhou, Fei Gao, Luqi Wang, Chuhao Liu, and Shaojie Shen. Robust and efficient quadrotor trajectory generation for fast autonomous flight. *IEEE Robotics and Automation Letters*, 4(4):3529–3536, 2019. DOI: 10.1109/LRA.2019.2927938.

[8] Christoph Krammer, Felix Schweighofer, Daniel Gierszewski, Simon Scherer, Tuğba Akman, Haichao Hong, and Florian Holzapfel. Requirements-based generation of optimal vertical takeoff and landing trajectories for electric aircraft. In *33rd Congress of the International Council of the Aeronautical Sciences (ICAS). ICAS*, 2022.

[9] Lester E Dubins. On curves of minimal length with a constraint on average curvature, and with prescribed initial and terminal positions and tangents. *American Journal of mathematics*, 79(3):497–516, 1957. DOI: 10.2307/2372560.

[10] Giuseppe Ambrosino, Marco Ariola, Umberto Ciniglio, Federico Corraro, Alfredo Pironti, and M Virgilio. Algorithms for 3d uav path generation and tracking. In *Proceedings of the 45th IEEE Conference on Decision and Control*, pages 5275–5280. IEEE, 2006. DOI: 10.1109/CDC.2006.377555.

[11] Kenneth Renny Simba, Naoki Uchiyama, and Shigenori Sano. Real-time smooth trajectory generation for nonholonomic mobile robots using bézier curves. *Robotics and Computer-Integrated Manufacturing*, 41:31–42, 2016. DOI: 10.1016/j.rcim.2016.02.002.

[12] Cheng Chen, Yuqing He, Chunguang Bu, Jianda Han, and Xuebo Zhang. Quartic bézier curve based trajectory generation for autonomous vehicles with curvature and velocity constraints. In *2014 IEEE International Conference on Robotics and Automation (ICRA)*, pages 6108–6113. IEEE, 2014. DOI: 10.1109/ICRA.2014.6907759.

[13] Xi Yu, Wenjun Zhu, and Li Xu. Real-time motion planning and trajectory tracking in complex environments based on bézier curves and nonlinear mpc controller. In *2020 Chinese Control And Decision Conference (CCDC)*, pages 1540–1546. IEEE, 2020. DOI: 10.1109/CCDC49329.2020.9163994.

[14] Doran K Wilde. Computing clothoid segments for trajectory generation. In *2009 IEEE/RSJ international conference on intelligent robots and systems*, pages 2440–2445. IEEE, 2009. DOI: 10.1109/IROS.2009.5354700.

[15] Volker Schneider, Patrick Piprek, Simon P Schatz, Thäddaus Baier, Christoph Dörhöfer, Markus Hochstrasser, Agnes Gabrys, Erik Karlsson, Christoph Krause, Patrick J Lauffs, et al. Online trajectory generation using clothoid segments. In *2016 14th International Conference on Control, Automation, Robotics and Vision (ICARCV)*, pages 1–6. IEEE, 2016. DOI: 10.1109/ICARCV.2016.7838711.

[16] P Piprek. Clothoid development for a trajectory system. Master's thesis, Technical University of Munich, 2014.

[17] Mohanad Alnuaimi. Performance comparison of clothoid and dubins path generation algorithms. In *AIAA AVIATION 2022 Forum*, page 3972, 2022. DOI: 10.2514/6.2022-3972.

[18] Volker Schneider and Florian Holzapfel. Modular trajectory generation test platform for real flight systems. In *Advances in Aerospace Guidance, Navigation and Control: Selected Papers of the Fourth CEAS Specialist Conference on Guidance, Navigation and Control Held in Warsaw, Poland, April 2017*, pages 185–202. Springer, 2018.

[19] ICAO. Doc 8168–procedures for air navigation services - aircraft operations (pans-ops), 2006.

[20] Erik Karlsson, Simon P Schatz, Thaddäus Baier, Christoph Dörhöfer, Agnes Gabrys, Markus Hochstrasser, Christoph Krause, Patrick J Lauffs, Nils C Mumm, Kajetan Nürnberger, et al. Automatic flight path control of an experimental da42 general aviation aircraft. In *2016 14th International Conference on Control, Automation, Robotics and Vision (ICARCV)*, pages 1–6. IEEE, 2016. DOI: 10.1109/ICARCV.2016.7838566.

[21] Simon P Schatz, Volker Schneider, Erik Karlsson, Florian Holzapfel, Thaddäus Baier, Christoph Dörhöfer, Markus Hochstrasser, Agnes Gabrys, Christoph Krause, Patrick J Lauffs, et al. Flightplan flight tests of an experimental da42 general aviation aircraft. In *2016 14th International Conference on Control, Automation, Robotics and Vision (ICARCV)*, pages 1–6. IEEE, 2016. DOI: 10.1109/ICARCV.2016.7838646.

[22] Pranav Bhardwaj, Stefan A Raab, Jiannan Zhang, and Florian Holzapfel. Integrated reference model for a tilt-rotor vertical take-off and landing transition uav. In *2018 Applied Aerodynamics Conference*, page 3479, 2018. DOI: 10.2514/6.2018-3479.

[23] Hannes Hofsäß, Barzin Hosseini, Julian Rhein, and Florian Holzapfel. On the design and model-based validation of flight control system automation for an unmanned coaxial helicopter. In *Software Engineering 2023 Workshops*. Gesellschaft für Informatik eV, 2023. DOI: 10.1109/DASC52595.2021.9594390.

[24] Valentin A Marvakov and Florian Holzapfel. A framework for simulation and formal verification of redundant flight control systems with components subject to partially synchronous timing effects. In *2021 IEEE/AIAA 40th Digital Avionics Systems Conference (DASC)*, pages 1–10. IEEE, 2021.

[25] Volker Schneider. *Trajectory Generation for Integrated Flight Guidance*. PhD thesis, Technische Universität München, 2018.

[26] David Seiferth, Benedikt Grüter, Matthias Heller, and Florian Holzapfel. Fully-automatic geofencing module for unmanned air systems in two dimensional space. In *AIAA Scitech 2019 Forum*, page 2078, 2019. DOI: 10.2514/6.2019-2078.

[27] ARINC Specification. 424-20: Navigation system database. aeronautical radio, 2011.

[28] Simon Scherer, Chinmaya Mishra, and Florian Holzapfel. Extension of the capabilities of an automatic landing system with procedures motivated by visual-flight-rules. In *33rd Congress of the International Council of the Aeronautical Sciences (ICAS)*, 2022.

[29] Simon Scherer, Moritz Speckmaier, Daniel Gierszewski, Chinmaya Mishra, Agnes Christine Steinert, Simona Wulf, Florian Holzapfel, et al. Automatic take-off and landing of a very light all electric optionally piloted aircraft. In *33rd Congress of the International Council of the Aeronautical Sciences (ICAS)*, 2022.

[30] Patrick Piprek, HONG Haichao, and Florian Holzapfel. Optimal trajectory design accounting for the stabilization of linear time-varying error dynamics. *Chinese Journal of Aeronautics*, 35(7):55–66, 2022. DOI: 10.1016/j.cja.2021.10.031.

[31] Simon P Schatz and Florian Holzapfel. Nonlinear modular 3d trajectory control of a general aviation aircraft. In *Advances in Aerospace Guidance, Navigation and Control: Selected Papers of the Fourth CEAS Specialist Conference on Guidance, Navigation and Control Held in Warsaw, Poland, April 2017*, pages 163–183. Springer, 2018.

[32] Agnes Steinert, Rasmus Steffensen, Daniel Gierszewski, Moritz Speckmaier, Florian Holzapfel, Robert Schmoldt, Frank Demmler, Ulrich Schell, Markus Ornigg, and Marius Koop. Experimental results of flight test based gain tuning. In *AIAA SCITECH 2022 Forum*, page 2296, 2022. DOI: 10.2514/6.2022-2296.

[33] Stanislav Braun, Markus Geiser, Matthias Heller, and Florian Holzapfel. Configuration assessment and preliminary control law design for a novel diamond-shaped uav. In *2014 International Conference on Unmanned Aircraft Systems (ICUAS)*, pages 1009–1020. IEEE, 2014. DOI: 10.1109/ICUAS.2014.6842352.

[34] Simon P. Schatz, Agnes C. Gabrys, Daniel M. Gierszewski, and Florian Holzapfel. Inner loop command interface in a modular flight control architecture for trajectory flights of general aviation aircraft. In *2018 5th International Conference on Control, Decision and Information Technologies (CoDIT)*, pages 86–91, 2018. DOI: 10.1109/CoDIT.2018.8394801.

[35] Leonhard Euler. Recherches sur la courbure des surfaces. *Mémoires de l'Académie des Sciences de Berlin*, pages 119–143, 1767.

[36] James R Clynch. Radius of the earth-radii used in geodesy. *Naval Postgraduate School*, 2002.

[37] Daniel C Alexander and Geralyn M Koeberlein. *Elementary geometry for college students*. Cengage Learning, 2014.

[38] Thomas Little Heath et al. *The thirteen books of Euclid's Elements*. Courier Corporation, 1956.

[39] Euclid. *Euclid's Elements*. Printed by Erhard Ratdolt, 300 BC.

[40] Daniel M Gierszewski, Volker Schneider, Patrick J Lauffs, Lars Peter, and Florian Holzapfel. Clothoid-augmented online trajectory generation for radius to fix turns. *IFAC-PapersOnLine*, 51(9):174–179, 2018. DOI: 10.1016/j.ifacol.2018.07.029.

[41] Konstantin Dmitriev, Shanza Ali Zafar, Kevin Schmiechen, Yi Lai, Micheal Saleab, Pranav Nagarajan, Daniel Dollinger, Markus Hochstrasser, Florian Holzapfel, and Stephan Myschik. A lean and highly-automated model-based software development process based on do-178c/do-331. In *2020 AIAA/IEEE 39th Digital Avionics Systems Conference (DASC)*, pages 1–10. IEEE, 2020. DOI: 10.1109/DASC50938.2020.9256576.